



Article

Conversion of Cr(VI) to Cr(III) in Water Using Amino-Modified Ordered Mesoporous Silicas: Influence of the Functional Group Architecture

Enrique Rodríguez-Castellón 1,* Daniel Ballesteros-Plata 1 and Nicolas Fellenz 1,2,*

- Departamento de Química Inorgánica, Cristalografía y Mineralogía, Facultad de Ciencias, Instituto de Investigación en Biorrefinerías I3B, Universidad de Málaga, Campus de Teatinos, 29071 Málaga, Spain; daniel.ballesteros@uma.es
- ² Laboratorio de Materiales Nanoestructurados (CONICET-UNRN), Rotonda Cooperación y Ruta Provincial N°1, Viedma 8500, Río Negro, Argentina
- * Correspondence: castellon@uma.es (E.R.-C.); nfellenz@unrn.edu.ar (N.F.)

Abstract

Two nitrogen-modified mesoporous MCM-41-type silicas were synthesized by the solgel route and post-grafting surface modification procedure, obtaining an aminopropylmodified MCM-41 (denoted MCM-41-N) and an aminoethyl-aminopropyl-modified MCM-41 (denoted MCM-41-NN). Hexavalent chromium removal from acidified water by adsorption and reduction to Cr(III) on the solid mesophases was analyzed. The modified silicas were characterized by powder X-ray diffraction (XRD), Fourier transformed infrared spectra (FT-IR), nitrogen adsorption-desorption measurements at -196 °C, X-ray photoelectron spectroscopy (XPS), ²⁹Si solid state Nuclear Magnetic Resonance (²⁹Si-RMN), and thermogravimetric analysis (TGA). Both samples exhibited very high capacities for decreasing Cr(VI) concentrations in water, according to the Langmuir isotherm model: 129.9 $\rm mg\cdot g^{-1}$ for MCM-41-N and 133.3 $\rm mg\cdot g^{-1}$ for MCM-41-NN. The chromium speciation in the supernatant after 24 h indicates that MCM-41-N had a higher capacity to reduce Cr(VI) to the less toxic Cr(III) species than MCM-41-NN: 92.9% vs. 72.5% when the initial Cr(VI) concentration was $10 \text{ mg} \cdot \text{g}^{-1}$. These differences were related to the different capacity of nitrogen atoms in MCM-41-N and MCM-41-NN to interact with the surrounding surface silanols which are required for the chemical reduction in the hexavalent species to take place, as evidenced by FT-IR and XPS analysis. Also, the Cr(III)/Cr(VI) atomic ratios on the solid's surfaces were higher for MCM-41-N. These results highlight the characteristics that nitrogen atoms incorporated into silica matrices must possess in order to maximize the transformation of Cr(VI) into the trivalent species, thereby reducing the generation of toxic waste harmful to living organisms.

Keywords: hexavalent chromium; adsorption; reduction; nitrogen-doped; silicas; water



Academic Editor: Francis Verpoort

Received: 8 July 2025 Revised: 20 August 2025 Accepted: 25 August 2025 Published: 26 August 2025

Citation: Rodríguez-Castellón, E.; Ballesteros-Plata, D.; Fellenz, N. Conversion of Cr(VI) to Cr(III) in Water Using Amino-Modified Ordered Mesoporous Silicas: Influence of the Functional Group Architecture. *Appl. Sci.* 2025, *15*, 9370. https://doi.org/ 10.3390/app15179370

Copyright: © 2025 by the authors. Licensee MDPI, Basel, Switzerland. This article is an open access article distributed under the terms and conditions of the Creative Commons Attribution (CC BY) license (https://creativecommons.org/licenses/by/4.0/).

1. Introduction

Ordered mesoporous silica, known as MCM-41, is, due to its outstanding chemical and structural characteristics, one of the most widely studied and utilized materials in the fields of catalysis and the separation of species of environmental and industrial interest [1,2]. The possibility of incorporating various chemical functionalities on its surface using organic functionalizing agents leads to organic-inorganic composite materials that combine, in a single solid phase, the properties of the rigid mesoporous network of silica with the specific

Appl. Sci. 2025, 15, 9370 2 of 18

chemical reactivity of the organic component. As a result, the surface functionalization of the MCM-41 system with silanes containing groups such as carboxylic acids, methyl, amines, sulfur atoms, phenanthroline, among others, resulted in long-lifetime silica-based solids capable of separating and/or catalyzing diverse compounds immersed in aqueous matrices of varying complexity [3–5].

Regarding the treatment of aqueous effluents containing hexavalent chromium (Cr(VI)), it has been shown that the covalent anchoring of amino-terminal functional groups onto the mesopore walls in the MCM-41 system produces a composite material with high Cr(VI) removal efficiency [6]. When the pH of the aqueous solution is close to neutrality, Cr(VI) ions exist predominantly as CrO₄²⁻, while the surface of amino-functionalized MCM-41 contains numerous positive charges, as the pKa of these organic functionalities falls within the pH range 9–10 [7,8]. Therefore, at pH \approx 7, electrostatic attraction occurs between the mesoporous system's surface and the negatively charged Cr(VI) species, resulting in an adsorption capacity that can exceed 60 mg·g $^{-1}$ [9]. In contrast, when the aqueous solution containing Cr(VI) is acidified, the chromium removal mechanism becomes more complex. Under these conditions, the predominant Cr(VI) species is HCrO₄⁻, while the surface of the amino-MCM-41 system is highly positive due to almost complete protonation of the amino species [10]. Thus, an initial step involving the adsorption of hexavalent chromium occurs, followed by a second step in which its reduction to Cr(III) occurs [6,11]. This combined adsorption-reduction process is more efficient when performed in an aqueous solution with a pH between 2 and 4 [12]. In a previous work, we demonstrated that for the reduction step to occur, the existence of a group adjacent to the HCrO₄⁻---NH³⁺ complex which is capable of interacting with the adsorbed Cr(VI) is essential [10]. In the case of N-doped MCM-41-based systems, the adjacent groups are the remaining silanols located near the inserted organic functionalities. When the silanols adjacent to the electrostatically generated acidic chromate-ammonium complex cannot interact with it, no reduction in Cr(VI) to Cr(III) is observed, and only Cr(VI) removal via adsorption occurs. Similarly, on nanostructured carbons doped with different types of N (i.e., pyrrolic and pyridinic) and using XPS measurements along with first-principles calculations, Ko et al. confirmed the need of a proton-donating group adjacent to the N atoms that retains the chromate for reduction to take place [13]. In the case of carbon-based materials, it is an alcohol group that releases a proton to initiate a mechanism similar to the Jones Oxidation Reaction, catalyzing the formation of Cr(III). Modification of MCM-41 with S-containing groups also enables the combined adsorption–reduction mechanism, but the synthesis of the MCM-41-SH/SO₃H system is more complex due to its higher number of steps compared to the MCM-41-N system [14]. Additionally, S-based groups do not have the advantage of being obtained from abundant and low-cost natural sources, like amino groups, which can be derived from chitin, one of the most abundant polymers in nature [15,16].

The importance of studying and developing processes to remove chromium lies in the fact that it is a metal widely used in industry, and as a result, it is released into the environment through leaks, poor storage, or inadequate treatment of effluents [17–19]. While Cr(VI) has high mobility in the environment and is highly toxic due to its mutagenic and teratogenic properties, Cr(III) has relatively low toxicity and limited mobility under mildly alkaline or acidic conditions. According to the USEPA (United States Environmental Protection Agency), the maximum permissible concentrations for industrial aqueous effluents are 0.1 and 2.0 mg·mL⁻¹ for Cr(VI) and total chromium, respectively [20]. Therefore, processes and/or materials that maximize the separation of Cr(VI) species along with their chemical transformation into less toxic trivalent species should be developed and used for the treatment of aqueous matrices containing this heavy metal, thus minimizing the generation of highly toxic waste that requires a final disposal stage to complete effluent

Appl. Sci. 2025, 15, 9370 3 of 18

treatment. Various techniques have been employed to mitigate the detrimental effects of Cr(VI), including chemical extraction, reverse osmosis, electrokinetic remediation, bioleaching, adsorption and ion exchange. However, adsorption-based processes are highly advantageous compared to other methods, as they not only offer low operational costs with high efficiencies, but also could have the ability to remove Cr(VI) and transform it into Cr(III) [11–13]. Despite these, little is known about how the structural architecture of nitrogen-containing functional groups influences the adsorption-reduction mechanism on mesoporous silica surfaces.

In this context, the aim of this work is to elucidate the relationship between the type of nitrogen-containing functional group anchored on MCM-41 and its Cr(VI) reduction efficiency, contributing new insights into the mechanism of this environmentally relevant water remediation process. To this end, mesoporous MCM-41 was synthesized and functionalized with organic agents that introduce different types of nitrogen atoms. Through an exhaustive characterization of the solids using FT-IR, XPS, low-angle XRD and TGA, we evaluated how the functional group architecture influences the ability of these materials to adsorb and reduce Cr(VI) in acidic aqueous media.

2. Materials and Methods

2.1. Reactants

Analytical grade reagents were used as received from Sigma-Aldrich (St. Louis, MO, USA). Hexadecyltrimethyl-amonnium bromide (CTAB, \geq 98%) was used as template directing agent, tetraethyl orthosilicate (TEOS, \geq 99%) was used as silica source, and surface modifications procedures were carried out using aminopropyl-triethoxysilane (APTES, \geq 98%) and N-(2-aminoethyl)-3-aminopropyltrimethoxysilane silane (AeAPTES, \geq 98%). Besides commercial toluene, absolute ethanol, potassium dichromate, hydrochloric acid and aqueous ammonia were other reagents used for the synthesis and adsorption tests.

2.2. Synthesis of MCM-41-Based Solids

The synthesis of the MCM-41 phase was carried out following the procedure of Grün et al., which is a variation of the well-known Stöber synthesis for monodispersed silica spheres [21]. Briefly, using the sol-gel method, a solution with a molar composition of 1 TEOS: 0.3 CTMABr: 11 NH₃: 58 ethanol: 144 H₂O, was formed, and the mixture was kept at 38 °C under magnetic stirring for 2 h. The resulting white precipitate was filtered off and washed repeatedly with distilled water. The mesoporous structure-directing agent was removed by calcination in air at 550 °C for 120 min with a heating rate of 2 °C·min⁻¹. The final sample was designated as MCM-41. The incorporation of functional groups containing nitrogen atoms to MCM-41 was carried out by means of a post-synthesis treatment on the calcined sample: after drying the sample in an oven for 24 h, 500 mg were placed in 50 mL of a solution of the selected functionalizing agent in toluene (1% v/v). With the aim of achieving a high degree of surface functionalization and in accordance with previous studies conducted by our group and other researchers, the molar ratio of functionalizing agent and MCM-41 was 4.3 and 4.6 for APTES and AeAPTES, respectively [6,11]. Postsynthesis treatments were performed for 6 h at 80 °C with magnetic stirring. Subsequently, the solids were separated by filtration and thoroughly washed with commercial ethanol. When APTES was used as the functionalizing agent, the final sample was designated as MCM-41-N, when AeAPTES was used, it was labeled as MCM-41-NN.

2.3. Characterization of MCM-41/N and MCM-41/NN

The long-range mesoporous ordering of the silica-based samples was analyzed by X-ray diffraction using standard automated powder X-ray diffraction equipment Appl. Sci. 2025, 15, 9370 4 of 18

(Philips PW 1710, Amsterdam, The Netherlands) provided with a diffracted-beam graphite monochromator and Cu K α radiation in the 20 range 1.5–8° with 0.02° steps and acquisition time of 2 s-step^{-1} . Fourier transformed infrared spectra of dry samples mixed with KBr (1:50 ratio) were obtained on a Nicolet iS5 Thermo-scientific spectrometer (Waltham, MA, USA) equipped with a Pike Diffuse IR cell with a resolution of 1 cm^{-1} . The textural properties, specific surface area (Sg), pore volume (Vp) and average pore diameter (Dp) were obtained from the nitrogen adsorption–desorption isotherms recorded at −196 °C on samples dried overnight at 100 °C under vacuum in a Micromeritics ASAP 2020 V1.02 E equipment (Norcross, GA, USA). The pore size distribution was determined using the Barret-Joyner-Halenda/Kruk-Jaroniec-Sashari method (BJH-KJS). The salt addition method was used to determine the surface charge variation as a function of pH and the point of zero charge (PZC). For this purpose, each sample was immersed in an aqueous NaCl solution with an initial pH fixed with HCl or NaOH (range 2-11). The pH variation after the addition of the selected sample was plotted against the initial pH value. Solid-state NMR spectra were carried out on a BRUKER High-Definition Nuclear Magnetic Resonance Spectrometer model AVIIIHD 600 (Billerica, MA, USA) with a magnetic field of 14.09 Tesla. The ²⁹Si analysis was carried out using the Hpdec technique, at a rotation speed of 15 kHz, with a decoupling sequence cw. Measurements were carried out on a DVT probe of 2.5 mm of triple resonance and double wideband range. Spectra were registered with 4200 scans. Measurements were carried out on an HXY, Efree Solid State Triple Resonance Probe of 3.2 mm. The spectra were registered with 100 scans. For ²⁹Si measurements, the D1 was 60 s. The surface composition of the samples was studied by X-ray photoelectron spectroscopy by a Physical Electronics PHI 5701 spectrometer (Chanhassen, MN, USA) with a non-monochromatic Mg-K α radiation (300 W, 15 kV, 1253.6 eV) and a multi-channel detector. The C 1s signal of adventitious carbon at 284.8 eV was used as a reference. Thermogravimetric analysis was used to measure the silane loading on the MCM-41 structure by means of a TA Instruments Mettler Toledo (Greifensee, Switzerland). The analysis was carried out by heating the functionalized samples up to 900 °C (10 °C·min⁻¹) in air flow $(40 \text{ mL} \cdot \text{min}^{-1}).$

2.4. Cr(VI) Removal Tests

To evaluate the capacity of the MCM-41-N and MCM-41-NN systems to adsorb Cr(VI) and reduce it to Cr(III), batch tests were carried out. For this purpose, aqueous solutions of Cr(VI) with varying concentrations (range 10–200 mg·L⁻¹) were prepared from K₂Cr₂O₇, the pH value was adjusted to 2 ± 0.2 by adding HCl and was monitored throughout the entire experiment. Then, 25 mg of the selected solid were added to 25 mL of each Cr(VI) solution under mechanical stirring. To ensure that equilibrium conditions were reached, after 24 h the solid was separated by centrifugation at $8000 \times g$ rpm for 15 min [12]. The final concentrations of Cr(VI) and Cr(III) in the supernatant were determined as follows: the total chromium concentration remaining in solution was measured by Inductively Coupled Plasma Optical Emission Spectrometry (ICP-OES) using a Shimadzu ICP-9000 instrument (Kyoto, Japan). The external calibration method was applied using certified standards from Chem-Lab, Zedelgem B-8210, Belgium, ultrapure nitric acid (sub-boiled) previously distilled with a Berghof distillacid BSB-939-IR distiller (GmbH, Eningen unter Achalm, Germany), and ultrapure water. To distinguish between Cr(VI) and Cr(III), Cr(VI) was determined by UV-Vis spectroscopy using a Shimadzu UV-1900i instrument at 540 nm, following the 1,5-diphenylcarbazide method [11]. The Cr(III) concentration in the supernatant was then calculated by subtracting the Cr(VI) concentration from the total chromium concentration. All assays were performed in triplicate, and the reported values represent the average of the data obtained.

Appl. Sci. 2025, 15, 9370 5 of 18

3. Results and Discussion

3.1. Characterization of MCM-41-N and MCM-41-NN

Figure 1 shows the results of DRX measurements. The diffractogram of MCM-41 exhibits a sharp and well-defined peak at 2.5°, along with two broader peaks in the range 4.0–5.5°. This diffractogram is typical of ordered mesoporous materials where the diffraction lines are generated by the presence of long-range pore ordering, and can be attributed to the 2D hexagonal p6m-type pore network typical of the hexagonal ordered mesoporous structure of MCM-41 (ICDD card number 00-049-1712) [21,22]. The functionalized samples exhibit diffractograms similar to that of the parent material with a slight decrease in the intensity of the peaks. This decrease is related to the difference in electron density between the silica walls and the functionalizing agents. The similarity in the X-ray diffraction patterns between MCM-41, MCM-41-N and MCM-41-NN indicates that the post-synthetic toluene treatments used to obtain the functionalized samples did not affect the original mesoporous structure.

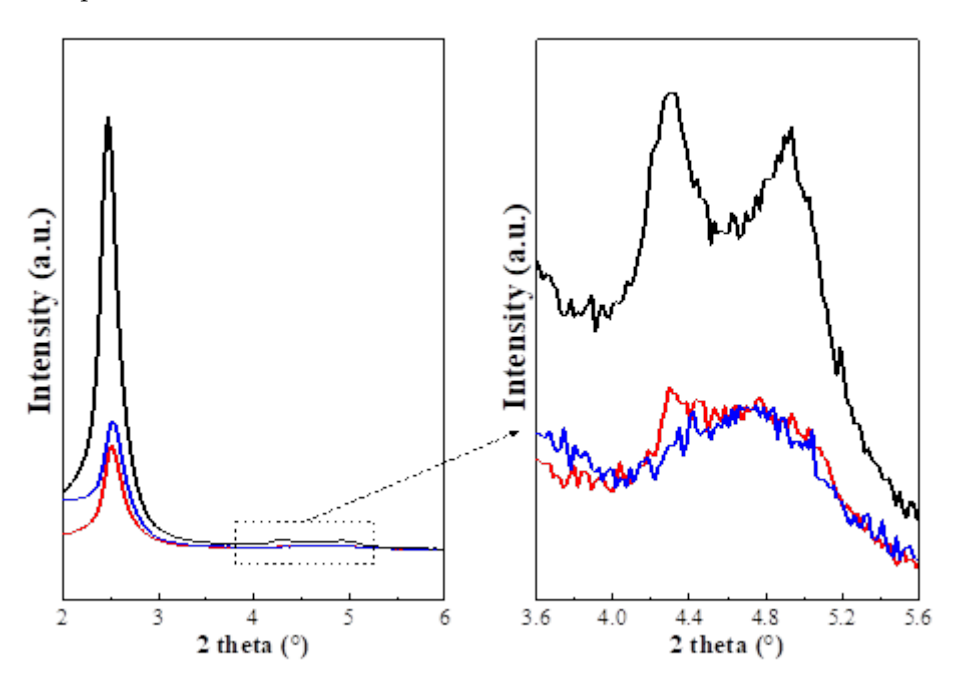


Figure 1. XDR patterns of MCM-41 (black), MCM-41-N (blue) and MCM-41-NN (red) and detail of the $4.0-5.0^{\circ}$ 2 theta region.

Figure 2 shows the infrared spectra of the pristine sample and its functionalized derivatives. The MCM-41 spectrum is dominated by a broad and intense band in the range 3800–2800 cm⁻¹, associated with stretching vibrations of OH-containing species: adsorbed water and surface hydroxyl groups [23]. Another intense and narrower band was observed in the range 1300–950 cm⁻¹, with a maximum at 1080 cm⁻¹, associated with vibrations typical of a Si-O-Si silicate network. Additionally, two bands of different intensity, but well-defined, are observed at 960 and 3745 cm⁻¹. These are associated with the vibrational modes of surface silanols (Si-OH). These species are present on the external surface of the particles, as well as decorating the internal surface formed by the mesopore walls. This spectrum is typical of pure ordered mesoporous silicas [23]. The spectra of the functionalized samples show marked differences compared to the MCM-41 spectrum. Neither MCM-41-N nor MCM-41-NN shows the bands associated with the presence of Si-OH: the band at 960 cm⁻¹ lost intensity and definition, becoming a shoulder on the main band at 1080 cm⁻¹, while the band at 3745 cm⁻¹ is barely visible. This indicates that the functionalization acted on the surface of the mesoporous system, using Si-OH species

Appl. Sci. 2025, 15, 9370 6 of 18

as anchoring points, as will be discussed later in the analysis of the ²⁹Si-NMR spectra. In the 3500–2800 cm⁻¹ region, a broadening is observed relative to the superposition of N-H stretching vibrations with those of OH-containing species. Furthermore, the presence of organic groups is confirmed by the appearance of weak bands in the 3000–2800 cm⁻¹ region, corresponding to C-H stretching vibrations, these bands being more intense in MCM-41-NN. The band at 1650 cm⁻¹, corresponding to the bending of adsorbed water molecules (δ O-H), is intense and narrow in MCM-41, whereas in the functionalized derivatives a broadening is observed due to the overlap with bands generated by the asymmetric bending of amino species [24]. Comparing the spectra of MCM-41-N and MCM-41-NN, it is observed that they do not present the same relative intensity between bands in the 1700–1600 cm⁻¹ region of the spectrum (Figure 2 inset). While MCM-41-NN presents a band at 1600 cm⁻¹ slightly more intense than that at 1630 cm⁻¹, MCM-41-N shows the opposite; the band at 1630 cm⁻¹, assignable to the asymmetric bending of $^+$ N-H, dominates this region of the spectrum, being more intense than that at 1600 cm $^{-1}$, which corresponds to the asymmetric bending of the deprotonated N-H species [24]. The same happens with the band corresponding to the asymmetric bending mode of ⁺N-H (1550 cm⁻¹) which presents higher relative intensity in MCM-41-N. This suggests that after synthesis, the amino species in the MCM-41-N sample has greater tendency to protonation than in MCM-41-NN. This type of protonation in as-synthesized functionalized silicas has been previously studied referring to it as the zwitterion salt model [25,26]. In this process, through the formation of a hydrogen bond involving the twisting of the organic chain, a residual silanol neighboring the grafted amino group reversibly donates a proton, resulting in the SiO^{δ-}H---^{δ+}NH₂ species. Although a more detailed study based on theoretical calculations would be required, the differences observed by FT-IR in terms of the degree of protonation could be due to the different steric hindrances presented by the aminopropyl residues compared to the aminoethyl-aminopropyl residues. That is, the longer organic chain anchored in MCM-41-NN would experience a greater strain to fold towards the surface, making interaction with a neighboring residual Si-OH less likely for protonation of the NH₂ groups. A more detailed discussion of the degree of protonation and the types of N atoms present in each sample will be presented in the XPS analysis.

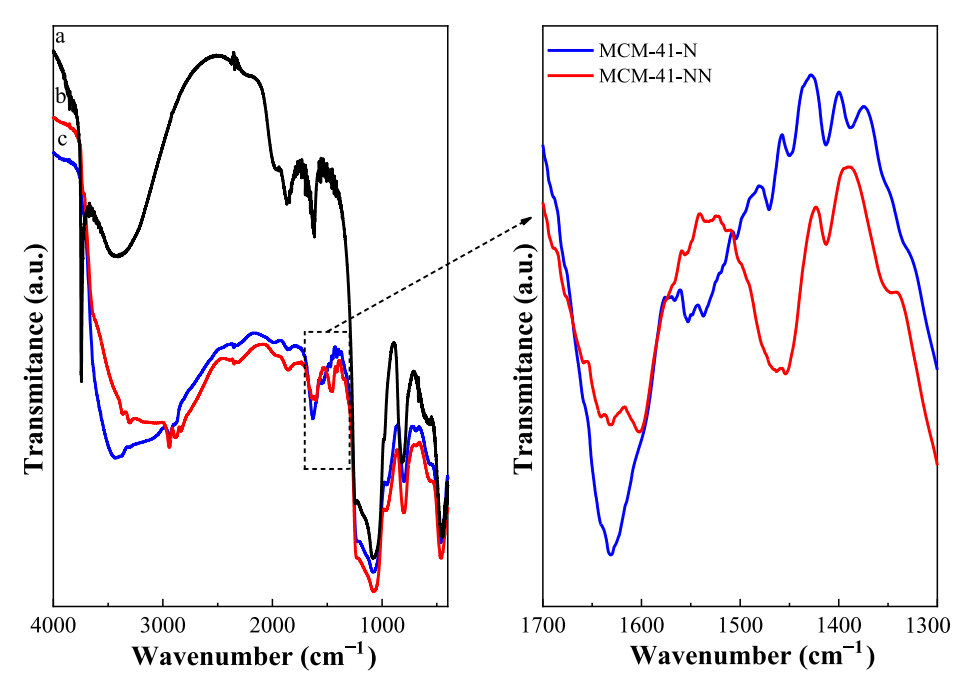


Figure 2. FT-IR spectra of MCM-41 (a—black), MCM-41-NN (b—red) and MCM-41-N (c—blue) and detail of the amino/ammonium associated vibrational modes signals (1700–1400 cm⁻¹ region).

Appl. Sci. 2025, 15, 9370 7 of 18

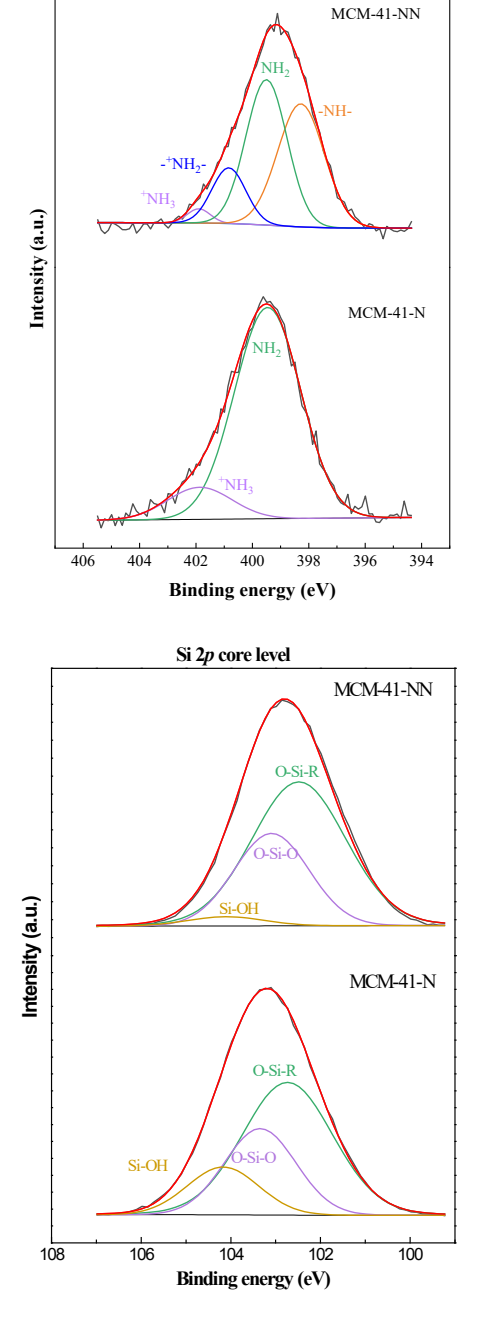
To obtain further details about the surface chemistry of fresh MCM-41-N and MCM-41-NN, XPS spectra of both as-synthesized samples were acquired (Figure 3). The highresolution N1s core level spectrum of MCM-41-N was fitted using two contributions at 401.9 and 399.5 eV, which were assigned to -+NH₃ and -NH₂, respectively [20,27]. The relative areas of each contribution indicate that the amino species predominates over the alkylammonium groups. For MCM-41-NN two additional contributions appeared compared to MCM-41-N. In addition to the signals corresponding to -NH₂ and -+NH₃ species, two bands appeared at 398.3 eV and 400.9 eV, which correspond to the free secondary amine (-NH-) and its protonated form (-+NH₂-) in the aminoethyl-aminopropyl anchored group, respectively [20]. It is important to highlight that the terminal - NH₃ species is present in minimal amounts in MCM-41-NN, 2.4% compared to 12.9% in MCM-41-N, consistent with the FT-IR results. Si 2p core spectra were deconvoluted into three contributions (Figure 3). For MCM-41-N, the higher energy band (104.2 eV) was assigned to the Si-OH species (15.5%). The band at 103.3 eV corresponds to the silicon atoms forming the walls of the mesoporous network (O-Si-O, 28%), and the lowest energy band (102.7 eV, 56.3%) was assigned to the Si atoms that are part of the functionalizing agent, i.e., O-Si-R, where R represents the anchored organic group [28]. For the fitting of the Si 2p spectrum for MCM-41-NN, the same three contributions were also obtained, although some differences in the intensity of the signals were observed. These differences indicate a higher presence of the Si-OH species in MCM-41-N (15.5%) compared to 3.2% in MCM-41-NN.

The ²⁹Si-NMR spectra for the functionalized samples are shown in Figure 4. Both spectra are dominated by a resonance signal at -110 ppm with a shoulder at -101 ppm. This indicates the predominant presence of the siloxane species (Si(SiO)₄), which forms the walls of MCM-41 and generates the resonance signal known as Q4 (-110 ppm), while the resonance at -101 ppm can be attributed to the remaining free silanols, denoted as Q3 [29,30]. Two additional signals are observed in the range of -50 to -80 ppm. The chemical shifts correspond to the so-called bidentate and tridentate structures: SiR(OR')(OSi)2 (-55 to -60 ppm; T2) and SiR(OSi)₃ (-60 to -70 ppm; T3), respectively, where R represents the organic functional group anchored onto the surface, i.e., aminopropyl or aminoethylaminopropyl. The presence of T2 and T3 signals and the absence of a resonance signal in the -45 to -50 ppm range indicate that the covalent anchoring of the functionalizing agents has occurred with two and three anchoring points [31]. It is also noteworthy that most of the T species are T3, demonstrating that the surface modification was efficient for both samples [32]. The T/(T + Q) area ratio is a semi-quantitative measure of the level of functionalization and/or the efficiency achieved in the surface functionalization process for modified silica materials. This parameter is 0.17 for MCM-41-N and 0.21 for MCM-41-NN, indicating that both samples have a similar degree of functionalization, with a slight improvement in efficiency for MCM-41-NN [32]. On the other hand, the Q3/Q4 ratio (0.32 and 0.19 for MCM-41-N and MCM-41-NN, respectively) indicates a higher presence of the Si-OH species in MCM-41-N compared to MCM-41-NN, consistent with the observations from XPS analysis.

Figure 5 shows the nitrogen sorption isotherms at $-196\,^{\circ}\text{C}$ of MCM-41 and its functionalized derivatives. All the isotherms are of type IV according to the IUPAC classification, indicating the presence of mesopores in all samples [33]. The absence of a hysteresis loop indicates that the mesopores have a diameter smaller than 4 nm, which was confirmed by applying the BJH-KJS model to obtain the pore size distribution (Figure 5b). The observed decrease in the average pore size for the functionalized samples, compared to MCM-41, can be explained by considering the different chain lengths of the functionalizing agents used, and the resulting thickening of the walls caused by each covalently anchoring to the porous system's walls. The BET surface area (S_g) and pore volume also show a decrease

Appl. Sci. 2025, 15, 9370 8 of 18

as a result of the functionalization process, with this effect being more pronounced in the MCM-41-NN sample, which exhibits a 38.9% drop in S_g compared to a 27.8% decrease in MCM-41-N relative to the initial value registered for MCM-41. The incorporation of the silanes onto MCM-41 surfaces also generated changes in the values of the constant C in the BET equation (Table 1). This parameter is related to the hydrophobicity/hydrophilicity character of the surfaces: a decrease in C indicates a reduced affinity for polar substances, such as water. Therefore, MCM-41-N and MCM-41-NN possess more hydrophobic surfaces than MCM-41, which is consistent with the observed decrease in the IR band corresponding to adsorbed water on the MCM-41-N and MCM-41-NN samples (Figure 2).



N 1s core level

Figure 3. High-resolution N 1*s* core level (**top**) and Si 2*p* core level (**bottom**) spectra of fresh MCM-41-N and MCM-41-NN.

Appl. Sci. 2025, 15, 9370 9 of 18

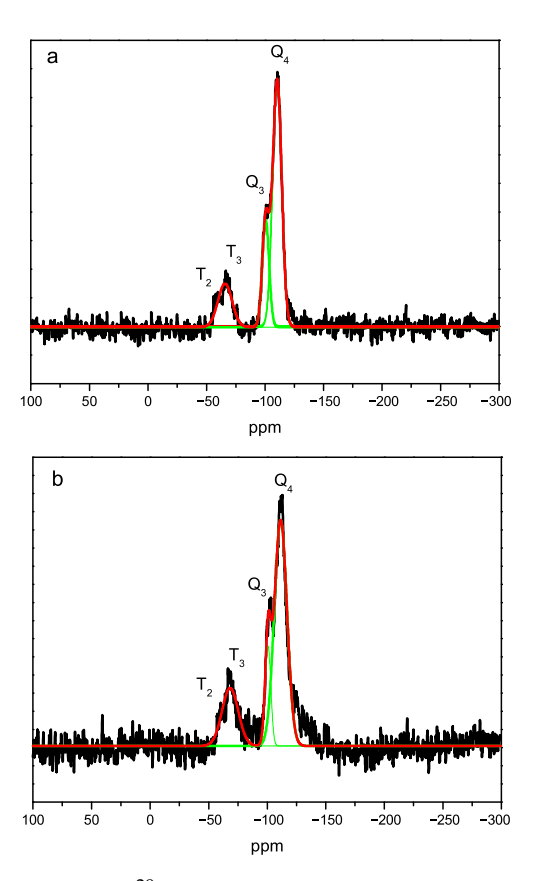


Figure 4. Si²⁹-RMN spectra of fresh MCM-41-N (**a**) and MCM-41-NN (**b**). Experimental data (black), fitting curves (red and green).

The acid-base behavior of the surface was analyzed using the salt addition method. This titration of a solid provides qualitative information on the species on the surface and allows the determination of the net surface charge at a specific pH value. Table 1 shows the pH values at which the surface of the samples no longer exchanges protons with the solution. These results indicate that the pristine MCM-41 system has a positively charged surface below pH = 3.1, due to the protonation of silanols, whose pKa is approximately 3.0. In aqueous solutions with pH \geq 3.1, the surface net charge becomes negative, indicating that the predominant species on the surface is SiO $^-$. For the functionalized samples, substantial changes in the acid-base behavior of the surface were observed. Both showed a marked increase in the measured PZC, indicating that the surface remains positive up to pH values of 8.6 and 8.1 for MCM-41-N and MCM-41-NN, respectively. Above these values, the net surface charge becomes negative. These changes result from the reversible protonation and deprotonation of the amino species incorporated during the functionalization processes (details in Supplementary Materials).

Table 1. Textural properties and nitrogen loadings of pristine MCM-41 and the hybrid mesoporous samples.

Sample/ Parameter	$Sg (m^2 \cdot g^{-1})^a$	Vp $(cm^3 \cdot g^{-1})^a$	Dp (nm) ^b	C ^a	Functional Group Loading $(mmol \cdot g^{-1})^{c}$	d (mmol·nm ⁻²)	PZC ^d
MCM 41	991	0.7	3.1	95.7	-	-	3.1
MCM 41-N	715	0.4	2.2	41.0	1.3	11.0	8.6
MCM 41-NN	605	0.3	2.0	39.5	1.5	14.9	8.1

^a by nitrogen sorption (BET), ^b BJH-KJS method, ^c by TGA measurements, ^d by salt addition method.

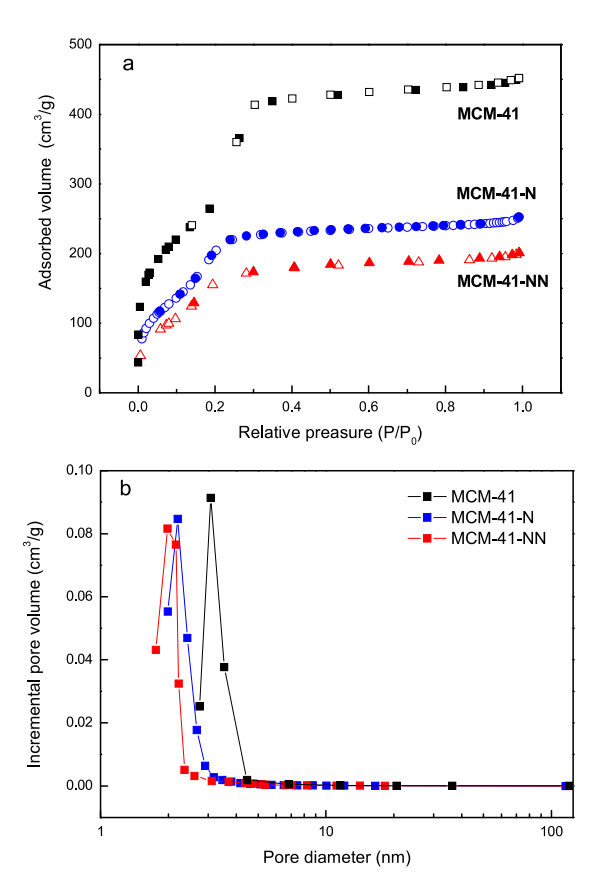


Figure 5. Nitrogen adsorption–desorption isotherms at -196 °C for MCM-41, MCM-41-N and MCM-41-NN (**a**) and pores sizes distribution in logarithmic scale obtained by applying BJH-KJS method (**b**).

The quantity of functional groups anchored to the surface of each sample was estimated through TGA (Figure 6). Although this technique does not allow an exact quantification of the organic groups grafted onto inorganic silica matrices, as the mass loss associated with the thermal degradation of organic functions partially overlaps with the mass loss due to the condensation of neighboring silanols, it does allow for a good comparison between functionalized OMSs. The weight loss from room temperature to 135 °C was attributed to the evaporation of physisorbed water, while the loss recorded between 200 and 800 °C was ascribed to the decomposition of the organic functions [29]. The weight loss due to water evaporation was very similar for MCM-41-N and MCM-41-NN, 4.8% and 5.3%, respectively, in accordance with the observations from the N₂ adsorption–desorption isotherms, where the C_{BET} constant values were quite similar for both samples. An integrated analysis of the results from TGA, BET, and FT-IR indicates that the incorporated amino functions generate higher surface hydrophobicity compared to pure MCM-41. Over the range of 200–800 °C, the percentage mass losses were 11.5% and 18.8% for MCM-41-N and MCM-41-NN, respectively, which corresponds to a loading of 1.3 mmol of aminopropyl per gram of MCM-41-N, versus 1.5 mmol of aminoethyl-aminopropyl per gram of MCM-41-NN. The density of functional groups on the surface (d), calculated using Equation (1) (Table 1), indicates a high degree of functionalization in both samples, suggesting that the incorporated functions are well dispersed throughout the mesoporous structure in agreement with Si²⁹-NMR findings [34].

$$d = N_A L_0 / S_{BET}$$
 (1)

where L_0 represents the number of molecules attached to the surface of the mesoporous silica, estimated by TGA, and S_{BET} is the specific surface area obtained from nitrogen sorption experiments.

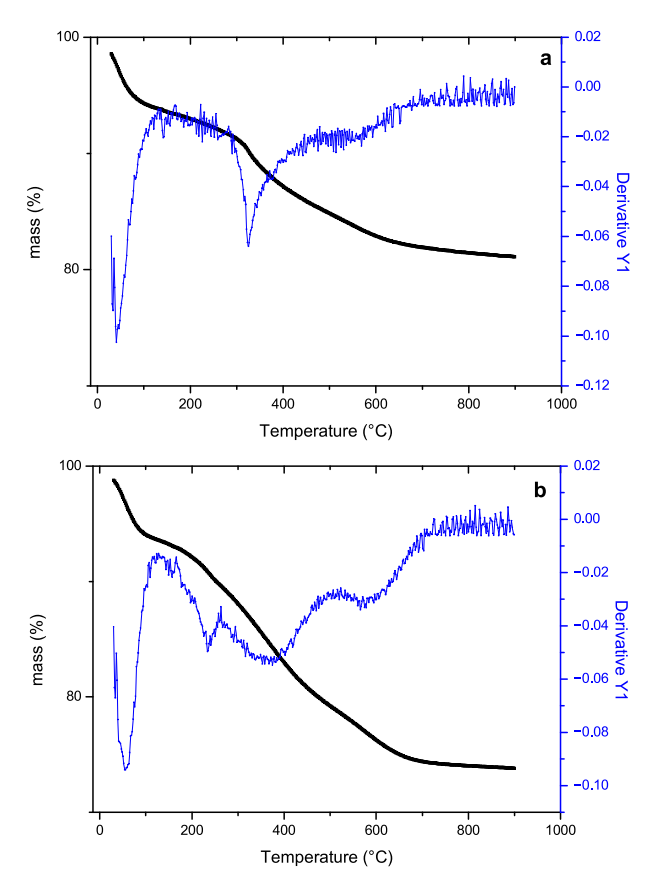


Figure 6. TGA profiles (black) and its first derivatives (blue) obtained in nitrogen atmosphere for MCM-41-N (**a**) and MCM-41-NN (**b**).

3.2. Performance of MCM-41-N and MCM-41-NN in Cr(VI) Removal

Figure 7a,b present the experimental data obtained from the Cr(VI) removal tests conducted in batch mode. On one hand, the amount of hexavalent chromium removed from the aqueous solution per gram of sample (q_e) is plotted against the concentration of hexavalent chromium remaining in the supernatant (C_e) for initial Cr(VI) concentrations ranging from 10 to 200 $mg \cdot L^{-1}$. Additionally, the total chromium adsorbed on the samples, determined by ICP-OES, is included in the graph. The experimental data were fitted to the Langmuir isotherm model (details of the fitting process in Supplementary Materials).

Removal tests conducted with pure MCM-41 indicate that the MCM-41/Cr(VI) interaction is negligible. For instance, when the initial Cr(VI) concentration was 130 mg·L $^{-1}$, the final chromium concentration after 24 h of contact under magnetic stirring at 20 °C was 128 mg·L $^{-1}$. All tests were performed at pH = 2 \pm 0.2, as previous studies have established this pH as optimal for maximizing chromium removal for aminofunctionalized OMSs [35,36]. Under these conditions, hexavalent chromium primarily exists as HCrO₄ $^-$ [9,37]. Since the surface of pure MCM-41 under these conditions is predominantly composed of Si-OH species, with small amounts of SiOH₂ $^+$ (as demonstrated by DLS/PZC measurements), it is understandable that the capacity of MCM-41 to remove Cr(VI) under acidic conditions is very low. In contrast, the functionalized samples exhibited very high capacities to remove Cr(VI) from water (Figure 7a, Table 2). The maximum capacities for Cr(VI) removal (q_m) obtained by fitting the experimental points to the Langmuir isotherm model were 129.9 mg·g $^{-1}$ for MCM-41-N and 133.3 mg·g $^{-1}$ for MCM-41-NN.

This suggests that the presence of aminopropyl or aminoethyl-aminopropyl groups does not result in significant differences in the final amount of Cr(VI) in the aqueous solution. However, when examining the final chromium concentrations in the supernatant separated into hexavalent and trivalent chromium, it is clear that while both samples exhibit similar capacities for Cr(VI) removal, they do so in different ways. Figure 7b shows the percentages of Cr(III) relative to total chromium in the supernatant. The amount of Cr(III) produced 24 h after contact of the initial solution with the solids is higher for MCM-41-N across the entire range of initial Cr(VI) concentrations evaluated, indicating that MCM-41-N has a higher capacity to reduce Cr(VI) to Cr(III) than MCM-41-NN. Thus, while the numerical capacity to decrease Cr(VI) concentrations is similar for both materials, MCM-41-N achieves this ability to remove Cr(VI) from water through a greater degree of progress in the reduction stage. Conversely, MCM-41-NN removes Cr(VI) from the aqueous solution with less reduction, suggesting that it adsorbs more Cr(VI) than it reduces. Finally, the q_m calculated considering the total chromium concentration in the supernatant was 107.1 and 122.1 $mg \cdot g^{-1}$ for MCM-41-N and MCM-41-NN, respectively. To understand these differences, it is essential to consider the mixed Cr(VI) adsorption-reduction mechanism proposed for silica-based materials containing nitrogen atoms. As mentioned above, this mechanism suggests that, in a first stage, an electrostatic interaction occurs between the negatively charged HCrO₄⁻ species and a surface ammonium ion. This process takes place in an acidic medium, followed by the formation of a hydrogen bond between a neighboring silanol and one of the oxygen atoms of the adsorbed chromate, which weakens the Cr-O bond and initiates the reduction to the trivalent species.

As demonstrated by FT-IR and XPS, the nitrogen atoms in MCM-41-N and MCM-41-NN do not have the same ability to interact with the surrounding silanols. This could be attributed to steric hindrance due to the differing chain lengths of the functionalizing groups. In this way, the lower ability of the aminoethyl-aminopropyl group to fold back on itself would hinder the proximity of the HCrO₄⁻ species to the neighboring silanol, thus reducing the ability of MCM-41-NN to reduce Cr(VI) to Cr(III), leaving the chromate predominantly adsorbed in the hexavalent state on the surface. In contrast, the greater ease of the aminopropyl group in forming the CrO---HO-Si hydrogen bond would favor the reduction stage. Similar results for Cr(VI) reduction were reported when Enterobacter sp. CTWI-06 was applied in one-stage batch culture shake flasks; this bacteria was recorded to reduce 58.89, 65.76, 76.34 and 84.65% of Cr(VI) but consuming up to 92 h and requiring large amounts of energy to maintain the optimal growth temperature of 37 °C [38]. On the other hand, zero-valent iron nanoparticles showed a low capacity to reduce hexavalent chromium along with a high tendency to oxidize due to dissolved oxygen in water; almost half of Cr(VI) remained in the solution when the initial Cr(VI) concentration was as low as $20 \text{ mg} \cdot \text{L}^{-1}$ and about 53% of chromium species on the sorbent surface were hexavalent [39]. Finally, it is important to highlight that amino-MCM-41 systems show a rapid initial adsorption of Cr(VI), which contrasts with the relatively longer times required by other solids such as iron nanoparticles and modified natural minerals, which typically require contact times ranging from minutes to hours [40,41].

Table 2. Chromium performance parameters obtained in bath assays at pH = 2.0 ± 0.2 at room temperature for nitrogen modified MCM-41 phases.

Sample/Parameter	$q_{m\ Cr(VI)}^{a}$ (mg·g ⁻¹)	$q_{m Cr(tot)}^{b}$ (mg·g ⁻¹)	Cr(III)/Cr(VI) c
MCM-41-N	129.9	107.1	1.1
MCM-41-NN	133.3	122.1	1.0

^a determined by applying the Langmuir model, ^b calculated from the differences between ICP-OES and UV-Vis chromium quantification in the supernatant, ^c over the surface samples determined by XPS.

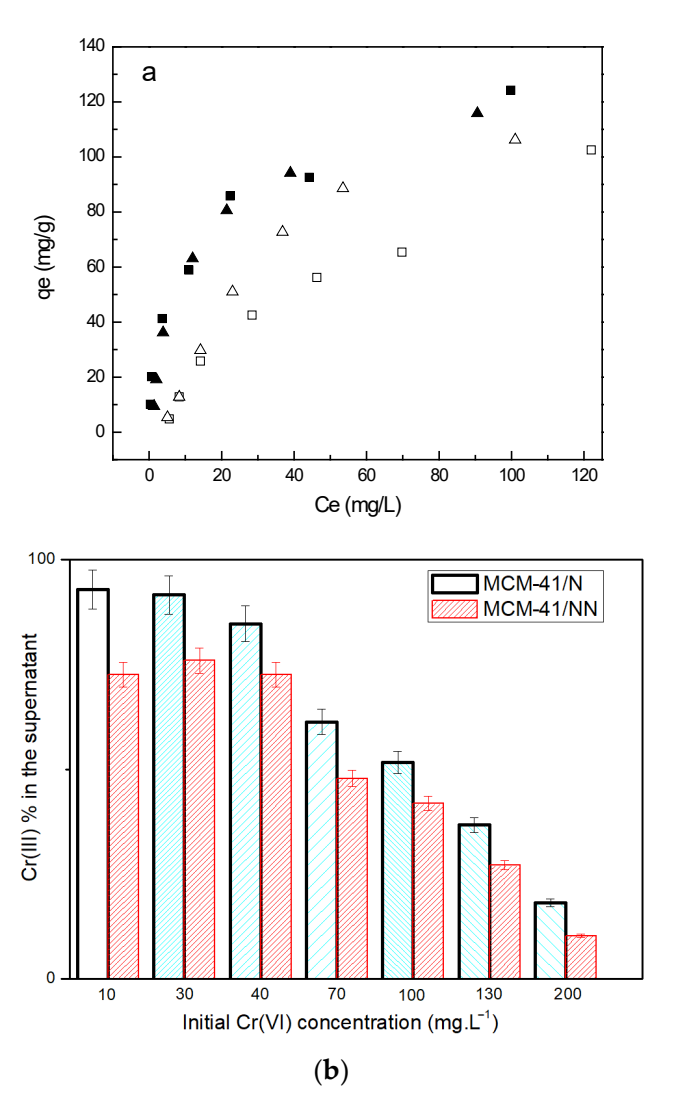


Figure 7. (a) Full adsorption isotherms for Cr(VI) removal in batch modality, pH = 2 ± 0.2 , T = $20\,^{\circ}$ C and 24 h contact time: MCM-41-N (filled black squares), MCM-41-NN (filled black triangles). Comparison with full adsorption isotherms considering total chromium concentration in the supernatant: MCM-41-N (empty squares), MCM-41-NN (empty triangles). (b) Cr(III) percentage in the final supernatant vs. Cr(VI) initial concentration between 10 and $200\,\text{mg}\cdot\text{L}^{-1}$.

3.3. Characterization of Used Samples

Samples after the sorption were analyzed by XPS in order to determine the chemical state of the chromium species on the mesophase surface. The high-resolution Cr 2*p* core level spectrum shows (Figure 8), in both modified MCM-41, two signals located at 575.9 and 577.7 eV, which correspond to Cr(III) and Cr(VI) species, respectively [27]. Analyzing the Cr(III)/Cr(VI) atomic ratio makes it possible to see the reduction capacity of each sorbent. Thereby the Cr(III)/Cr(VI) atomic ratios were 1.0 and 1.1 for MCM-41-NN and MCM-41-N, respectively, indicating a higher presence of trivalent chromium over the aminopropyl functionalized surface. This agrees with the greater reductive capacity observed in the adsorption tests, as indicated by the higher amount of trivalent chromium in the supernatant when MCM-41-N was used.

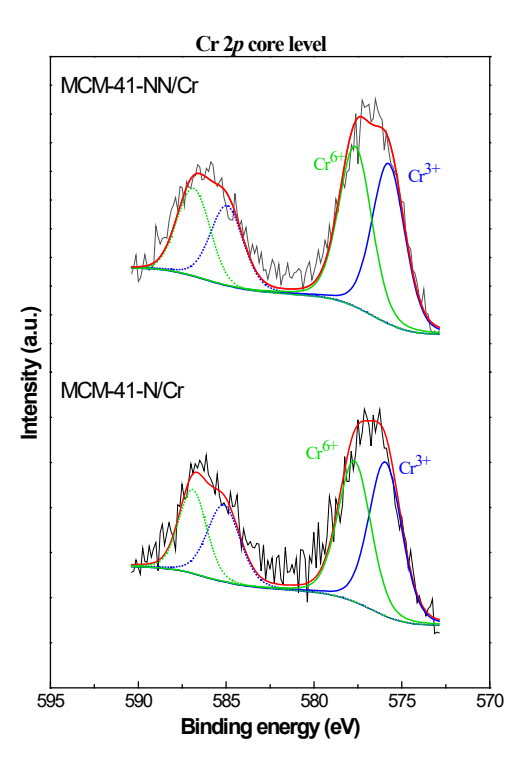


Figure 8. High-resolution Cr 2*p* core level spectra of chromium loaded MCM-41-N and MCM-41-NN.

The high-resolution O 1s core level spectra of the chromium-loaded samples were deconvoluted into three different contributions, one more than in the fresh samples (Figures S2–S5 in Supplementary Materials). The new signal that appears at lower binding energy (530.2 and 530.1 eV for used MCM-41-NN and MCM-41-N) corresponds to chromium oxides [42]. Additionally, a significant change was observed in the Si 2p binding energy region of the used samples compared to the fresh ones (Figures S6 and S7 in Supplementary Materials). The signal corresponding to the Si atoms of the organic group (102.5-102.7 eV) showed a decrease in intensity, dropping from 56.3% to 15.4% for MCM-41-N and from 64.5% to 15.3% for MCM-41-NN after contact with the Cr(VI) solution. This decrease could be attributed to the partial leaching of the organic functions anchored to the surface of the functionalized MCM-41 systems. A new peak appeared at lower binding energy, 102.3 eV for MCM-41-N and 101.9 eV for MCM-41-NN, accompanied by the disappearance of the signal corresponding to the Si-OH species, indicating that the surface silanols play an important role in the retention of chromium species onto the surface of the amino-functionalized MCM-41 systems. This observation is consistent with the findings in the high-resolution O 1s spectra of chromium-loaded samples, as the area of the O atoms of the silanol species decreases by the same amount as the area of the new peak corresponding to O-Cr (details in Supplementary Materials).

The high-resolution N 1s core level spectra of both used samples are shown in Figure 9. For MCM-41-N loaded with chromium, a significant shift to lower energies ($\Delta = -0.9 \, \mathrm{eV}$) was observed in the band assigned to the -+NH₃ species. In contrast, no shifts in the binding energies of nitrogen species were observed for used MCM-41-NN. The amino species decreased in presence while the ammonium increased, which is expected since the batch tests were performed under acidic conditions. The differences between the spectra of the spent samples indicate that the interaction with the chromate ion is much stronger when the organic group on the surface is aminopropyl against aminoethyl-aminopropyl, which would be related to the greater capacity of this group to reduce Cr(VI) to Cr(III).

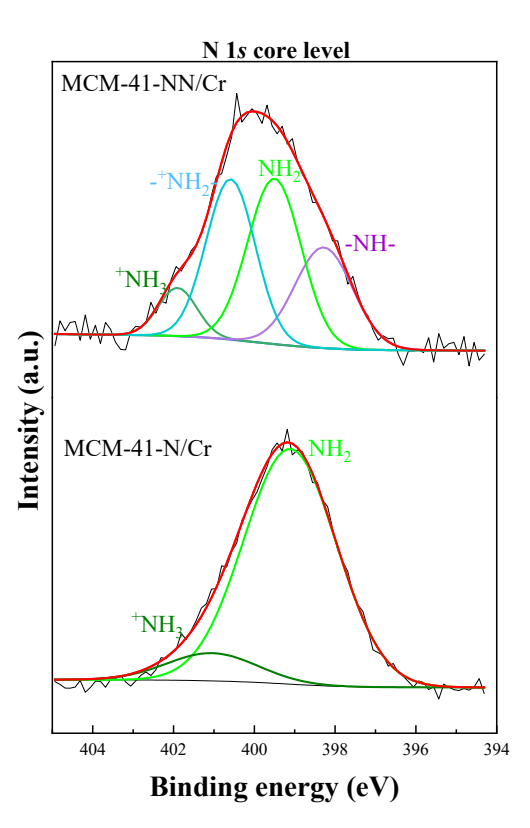


Figure 9. High resolution N 1s core level spectra of chromium-loaded MCM-41-N and MCM-41-NN.

4. Conclusions

Nitrogen-modified MCM-41 structures synthesized by the sol-gel route and postgrafting technique using toluene solutions of APTES or AeAPTES, showed high specific surface areas, greater than 600 m²·g⁻¹, long order mesopore arrangements with unimodal pore size distributions of 2.2 and 2.0 nm, and an organic functional group loading determined by TGA of around 1.3 mmol·g $^{-1}$. ²⁹Si-NMR experiments indicate that the covalent anchoring of the functionalizing agents has occurred with two and three anchoring points, generating a noticeable change in the acid-base behavior of the solids surface: the point-zerocharge shifted from 3.5 for the starting MCM-41 to 8.6 and 8.1 for the aminopropyl-MCM-41 and aminoethyl-aminopropyl-MCM-41, respectively. The terminal -*NH₃ species is present in minimal amounts in MCM-41-NN, 2.4% compared to 12.9% in MCM-41-N, indicating a greater tendency of the aminopropyl group in MCM-41-N to fold back onto itself and interact with the surface compared to the aminoethyl-aminopropyl group in MCM-41-NN, as evidenced by FT-IR and XPS measurements. Both samples demonstrated high Cr(VI) removal capabilities from aqueous solutions at pH 2, with q_m values above 125 mg·g⁻¹, as determined by the Langmuir isotherm model. However, MCM-41-N exhibited a superior ability to reduce Cr(VI) to Cr(III), which was related to the increased propensity of the aminopropyl group to fold itself towards the surface. Following an initial step, due to electrostatic interaction between the ammonium surface entities and aqueous hexavalent chromium, this folding facilitates the proximity of adsorbed chromate ions to the neighboring silanol groups, thereby promoting the reduction process. In contrast, the low ability of the aminoethyl-aminopropyl group to undergo similar folding restricts the proximity of the HCrO₄⁻ species to the neighboring silanols, limiting the occurrence of Cr(VI) reduction to Cr(III), so the chromate remains adsorbed on the sorbent surface.

Supplementary Materials: The following supporting information can be downloaded at https://www.mdpi.com/article/10.3390/app15179370/s1, Figure S1: Surface charge as a function of pH determined by the salt addition method for the functionalized samples; the intersection with the zero value on the

Y-axis denotes the PZC of each sample; Figure S2: High resolution O 1s XPS spectra of fresh MCM-41-N; Figure S3: High resolution O 1s XPS spectra of chromium loaded MCM-41-N; Figure S4: High resolution O 1s XPS spectra of fresh MCM-41-NN; Figure S5: High resolution O 1s XPS spectra of chromium loaded MCM-41-NN; Figure S6: High resolution Si 2p XPS spectra of chromium loaded MCM-41-N; Figure S7: High resolution Si 2p XPS spectra of chromium loaded MCM-41-NN; Table S1: Correlation parameters of isothermal adsorption Langmuir model for MCM-41-N and MCM-41-NN for the removal of Cr⁶⁺ from distilled water.

Author Contributions: Conceptualization, N.F. and E.R.-C.; methodology, N.F. and E.R.-C.; software, N.F. and D.B.-P.; validation, N.F. and D.B.-P.; formal analysis, N.F. and D.B.-P.; investigation, N.F., D.B.-P. and E.R.-C.; resources, N.F. and E.R.-C.; data curation, N.F. and D.B.-P.; writing—original draft preparation, N.F.; writing—review and editing, N.F., D.B.-P. and E.R.-C.; visualization, N.F., D.B.-P. and E.R.-C.; supervision, N.F., D.B.-P. and E.R.-C.; project administration, N.F. and E.R.-C.; funding acquisition, N.F. and E.R.-C. All authors have read and agreed to the published version of the manuscript.

Funding: This work was funded by Fundación Williams, Agencia Nacional de Promoción de la Investigación, el Desarrollo Tecnológico y la Innovación and Fundación YPF projects PI-40-1139 and PICT-005, and the Spanish Ministry of Science and Innovation, PID2021-126235OB-C32 funded by MCIN/AEI/10.13039/501100011033 and FEDER funds, and projects TED2021–130756B-C31 funded by MCIN/AEI/10.13039/501100011033 and by "ERDF A way of making Europe" by the European Union NextGeneration EU/PRTR.

Institutional Review Board Statement: Not applicable.

Informed Consent Statement: Not applicable.

Data Availability Statement: The original contributions presented in this study are included in the article/Supplementary Materials. Further inquiries can be directed to the corresponding author.

Acknowledgments: The authors would like to thank Ana Lucena Serrano and Elena Rodríguez Aguado for their valuable assistance in RMN and XPS measurements and Pedro Martín for facilitating the MCM-41 samples. N.F. is deeply grateful to all the staff of the Laboratorio de Catálisis from the University of Málaga for their great assistance and support during his stay in the Servicios Centrales de Apoyo a la Investigación.

Conflicts of Interest: The authors declare no conflict of interest.

References

- 1. Chai, Z.; Liu, B.; Lv, P.; Bai, Y.; Wang, J.; Su, W.; Song, X.; Yu, G.; Xu, G. Microwave synthesis of amino-functionalized MCM-41 from coal gasification fine slag for efficient bidirectional adsorption of anionic and cationic dyes. *Chemosphere* **2024**, 351, 141229. [CrossRef]
- Costa, J.A.S.; de Jesus, R.A.; Santos, D.O.; Mano, J.F.; Romão, L.P.C.; Paranhos, C.M. Recent progresses in the adsorption of organic, inorganic, and gas compounds by MCM-41-based mesoporous materials. *Microporous Mesoporous Mater.* 2020, 291, 109698.
 [CrossRef]
- 3. Freitas Cavalcante, J.C.; da Silva, A.M.; Batista Caldas, P.M.; de Sousa Barbosa, B.V.; da Silva Júnior, H.B.; Nicácio Alves, J.J. Characterization and optimization of biodiesel production from corn oil using heterogeneous MoO₃/MCM-41 catalysts. *Catal. Today* **2025**, *446*, 115119. [CrossRef]
- 4. Kuppireddy, S.; Varghese, A.M.; Araj, H.; Hart, P.; Ramantani, T.; Bampos, G.; Karanikolos, G.N. A combined experimental and simulations assessment of CO₂ capture and CO₂/H₂ separation performance of aminosilane-grafted MCM-41 and pore-expanded MCM-41. *Microporous Mesoporous Mater.* **2024**, *377*, 113220. [CrossRef]
- Vera-Baquero, F.L.; Morante-Zarcero, S.; Pérez-Quintanilla, D.; Sierra, I. Exploring Adsorption Performance of Functionalized Mesoporous Silicas with a Different Pore Structure as Strong Cation-Exchange Sorbents for Solid-Phase Extraction of Atropine and Scopolamine. *Appl. Sci.* 2025, 15, 646. [CrossRef]
- 6. Mallik, A.K.; Moktadir, A.; Rahman, A.; Shahruzzaman; Rahman, M.M. Progress in surface-modified silicas for Cr(VI) adsorption: A review. *J. Hazard. Mater.* **2022**, 423, 127041. [CrossRef]
- 7. Tandon, R.K.; Crisp, P.T.; Ellis, J.; Baker, R. Effect of pH on Chromium(VI) species in solution. Talanta 1984, 31, 227–228. [CrossRef]

8. Zhao, B.; Wang, Y.; Luo, X.; Luo, J.; Li, G.; Deng, L.; Cao, Y. Interfacial adsorption behavior of amine-functionalized MCM-41 for Mo(VI) capture from aqueous solution. *Environ. Res.* **2025**, *269*, 120821. [CrossRef]

- 9. Liao, P.; Li, B.; Xie, L.; Bai, X.; Qiao, H.; Li, Q.; Yang, B.; Liu, C. Immobilization of Cr(VI) on engineered silicate nanoparticles: Microscopic mechanisms and site energy distribution. *J. Hazard. Mater.* **2020**, *383*, 121145. [CrossRef]
- 10. Martin, P.; Rafti, M.; Marchetti, S.; Fellenz, N. MCM-41-based composite with enhanced stability for Cr(VI) removal from aqueous media. *Solid State Sci.* **2020**, *106*, 106300. [CrossRef]
- 11. Fellenz, N.; Perez-Alonso, F.J.; Martin, P.P.; García-Fierro, J.L.; Bengoa, J.F.; Marchetti, S.G.; Rojas, S. Chromium (VI) removal from water by means of adsorption-reduction at the surface of amino-functionalized MCM-41 sorbents. *Microporous Mesoporous Mater.* **2017**, 239, 138–146. [CrossRef]
- 12. Fellenz, N.; Martin, P.P.; Marchetti, S.G.; Bengoa, J.F. Aminopropyl-modified mesoporous silica nanospheres for the adsorption of Cr(VI) from water. *J. Porous Mater.* **2015**, 22, 729. [CrossRef]
- 13. Ko, Y.; Choi, K.; Lee, S.; Jung, K.; Hong, S.; Mizuseki, H.; Choi, J.; Lee, W. Strong chromate-adsorbent based on pyrrolic nitrogen structure: An experimental and theoretical study on the adsorption mechanism. *Water Res.* **2018**, *145*, 287–296. [CrossRef] [PubMed]
- 14. Zaitseva, N.; Zaitsev, V.; Walcarius, A. Chromium(VI) removal via reduction-sorption on bi-functional silica adsorbents. *J. Hazard. Mater.* **2013**, 250–251, 454–461. [CrossRef]
- Dong, X.; Shi, L.; Ma, S.; Chen, X.; Cao, S.; Li, W.; Zhao, Z.; Chen, C.; Deng, H. Chitin/Chitosan Nanofibers Toward a Sustainable Future: From Hierarchical Structural Regulation to Functionalization Applications. Nano Lett. 2024, 24, 12014–12026. [CrossRef]
- 16. Malinkina, O.; Shmakov, S.L.; Shipovskaya, A.B. Structure, the energy, sorption and biological properties of chiral salts of chitosan with l- and d-ascorbic acid. *Int. J. Biol. Macromol.* **2024**, 257, 128731. [CrossRef]
- 17. Nandi, R.; Laskar, S.; Saha, B. Surfactant-promoted enhancement in bioremediation of hexavalent chromium to trivalent chromium by naturally occurring wall algae. *Res. Chem. Intermed.* **2017**, *43*, 1619–1634. [CrossRef]
- 18. Ukhurebor, K.; Aigbe, U.O.; Onyancha, R.B.; Nwankwo, W.; Osibote, O.A.; Paumo, H.K.; Ama, O.M.; Adetunji, C.O.; Siloko, I.U. Effect of hexavalent chromium on the environment and removal techniques: A review. *J. Environ. Manag.* **2021**, 280, 111809. [CrossRef]
- 19. Karthik, C.; Barathi, S.; Pugazhendhiv; Ramkumar, V.S.; Thi, N.; Arulselvi, P.I. Characterization of multifarious plant growth promoting traits of rhizobacterial strain AR6 under Chromium(VI) stress. *Microbiol. Res.* **2017**, 204, 65–71. [CrossRef]
- 20. Wang, Q.; Zuo, W.; Tian, Y.; Kong, L.; Cai, G.; Zhang, H.; Li, L.; Zhang, J. An ultralight and flexible nanofibrillated cellulose/chitosan aerogel for efficient chromium removal: Adsorption-reduction process and mechanism. *Chemosphere* 2023, 329, 138622. [CrossRef]
- 21. Grün, M.; Unger, K.K.; Matsumoto, A.; Tsutsumi, K. Novel pathways for the preparation of mesoporous MCM-41 materials: Control of porosity and morphology. *Microporous Mesoporous Mater.* **1999**, *27*, 207–216. [CrossRef]
- Kruk, M.; Jaroniec, M.; Sakamoto, Y.; Terasaki, O.; Ryoo, R.; Ko, C.H. Determination of Pore Size and Pore Wall Structure of MCM-41 by Using Nitrogen Adsorption, Transmission Electron Microscopy, and X-ray Diffraction. J. Phys. Chem. B 2000, 104, 292–301. [CrossRef]
- 23. Kaur, P.; Chopra, H.K. SBA-15 supported benzoxazolium-based ionic liquids: Synthesis, characterization, and application in the adsorptive desulfurization. *Fuel Process. Technol.* **2022**, 238, 107480. [CrossRef]
- 24. Calvo, A.; Angelome, P.C.; Sanchez, V.M.; Scherlis, D.A.; Williams, F.J.; Soler-Illia, G.J.A.A. Mesoporous aminopropyl-functionalized hybrid thin films with modulable surface and environment-responsive behavior. *Chem. Mater.* **2008**, *20*, 4661–4668. [CrossRef]
- 25. Zhmud, B.V.; Sonnefeld, J. Aminopolysiloxane gels: Production and properties. J. Non Cryst. Solids 1996, 195, 16–27. [CrossRef]
- Walcarius, A.; Etienne, M.; Lebeau, B. Rate of Access to the Binding Sites in Organically Modified Silicates. 2. Ordered Mesoporous Silicas Grafted with Amine or Thiol Groups. Chem. Mater. 2003, 15, 2161–2173. [CrossRef]
- 27. Fang, L.; Zeng, J.; Wang, H.; He, F.; Wan, H.; Li, M.; Ren, W.; Ding, L.; Yang, L.; Luo, X. Insights into the proton-enhanced mechanism of hexavalent chromium removal by amine polymers in strong acid wastewater: Reduction of hexavalent chromium and sequestration of trivalent chromium. *J. Colloid Interface Sci.* 2023, 650, 515–525. [CrossRef]
- 28. Ko, Y.G.; Shin, S.S.; Choi, U.S. Primary, secondary, and tertiary amines for CO₂ capture: Designing for mesoporous CO₂ adsorbents. *J. Colloid Interface Sci.* **2011**, *361*, 594–602. [CrossRef]
- 29. Yismaw, S.; Ebbinghaus, S.G.; Wenzel, M.; Poppitz, D.; Gläser, R.; Matysik, J.; Bauer, F.; Enke, D. Selective functionalization of the outer surface of MCM-48-type mesoporous silica nanoparticles at room temperature. *J. Nanopart. Res.* **2020**, 22, 279. [CrossRef]
- Dogan, F.; Hammond, K.D.; Tompsett, G.A.; Huo, H.; Curtis Conner, W., Jr.; Auerbach, S.M.; Grey, C.P. Searching for Microporous, Strongly Basic Catalysts: Experimental and Calculated 29Si NMR Spectra of Heavily Nitrogen-Doped Y Zeolites. J. Am. Chem. Soc. 2009, 131, 11062–11079. [CrossRef]

31. Zúñiga, E.; Belmar, L.; Toledo, L.; Torres, C.; Rivas, B.L.; Sánchez, S.A.; Urbano, B.F. Rhodamine-loaded surface modified mesoporous silica particles embedded into a thermoresponsive composite hydrogel for prolonged release. *Eur. Polym. J.* **2017**, 95, 358–367. [CrossRef]

- 32. Miyajima, T.; Abry, S.; Zhou, W.; Albela, B.; Bonneviot, L.; Oumi, Y.; Sano, T.; Yoshitake, H. Estimation of spacing between 3-bromopropyl functions grafted on mesoporous silica surfaces by a substitution reaction using diamine probe molecules. *J. Mater. Chem.* **2007**, *17*, 3901–3909. [CrossRef]
- 33. Buttersack, C. General Cluster Sorption Isotherm. Microporous Mesoporous Mater. 2021, 316, 110909. [CrossRef]
- 34. Popova, M.; Szegedi, A.; Yoncheva, K.; Konstantinov, S.; Petrova, G.P.; Aleksandrov, H.A.; Vayssilov, G.N.; Shestakova, P. New method for preparation of delivery systems of poorly soluble drugs on the basis of functionalized mesoporous MCM-41 nanoparticles. *Microporous Mesoporous Mater.* **2014**, *198*, 247–255. [CrossRef]
- 35. Sun, Y.; Lyu, H.; Gai, L.; Sun, P.; Shen, B.; Tang, J. Biochar-anchored low-cost natural iron-based composites for durable hexavalent chromium removal. *Chem. Eng. J.* 2023, 476, 146604. [CrossRef]
- 36. Verma, R.; Maji, P.K.; Sarkar, S. Removal of hexavalent chromium from impaired water: Polyethylenimine-based sorbents—A review. *J. Environ. Chem. Eng.* **2023**, *11*, 109598. [CrossRef]
- 37. Losev, V.N.; Didukh-Shadrina, S.L.; Orobyeva, A.S.; Metelitsa, S.I.; Samoilo, A.S.; Zhizhaev, A.M.; Trofimchuk, A.K. Effective separation of chromium species in technological solutions using amino-immobilized silica prior to their determination. *J. Hazard. Mater.* **2021**, 407, 124383. [CrossRef]
- 38. Pattnaik, S.; Dash, D.; Mohapatra, S.; Pattnaik, M.; Marandi, A.K.; Das, S.; Samantaray, D.P. Improvement of rice plant productivity by native Cr(VI) reducing and plant growth promoting soil bacteria *Enterobacter cloacae*. *Chemosphere* **2020**, 240, 124895. [CrossRef]
- 39. Wu, J.; Yan, M.; Lv, S.; Yin, W.; Bu, H.; Liu, L.; Li, P.; Deng, H.; Zheng, X. Preparation of highly dispersive and antioxidative nano zero-valent iron for the removal of hexavalent chromium. *Chemosphere* **2021**, 262, 127733. [CrossRef]
- 40. Yang, X.; Zhou, Y.; Hu, J.; Zheng, Q.; Zhao, Y.; Lv, G.; Liao, L. Clay minerals and clay-based materials for heavy metals pollution control. *Sci. Total Environ.* **2024**, *954*, 176193. [CrossRef]
- 41. Abbou, B.; Lebkiri, I.; Ouaddari, H. Evaluation of Illitic-Kaolinite clay as an adsorbent for Cr³⁺ removal from synthetic aqueous solutions: Isotherm, kinetic, and thermodynamic analyses. *Chem. Phys. Impact* **2024**, *8*, 100527. [CrossRef]
- 42. Moulder, J.F.; Stickle, W.F.; Sobol, P.E.; Bomben, K.D. *Handbook of X-Ray Photoelectron Spectroscopy*; Chastain, J., Ed.; Perkin-Elmer Corporation: Eden Praire, MN, USA, 1992; ISBN 0-9627026-2-5.

Disclaimer/Publisher's Note: The statements, opinions and data contained in all publications are solely those of the individual author(s) and contributor(s) and not of MDPI and/or the editor(s). MDPI and/or the editor(s) disclaim responsibility for any injury to people or property resulting from any ideas, methods, instructions or products referred to in the content.